ACS OMEGA

http://pubs.acs.org/journal/acsodf

Article

Physicochemical Characteristics and Antibacterial Activities of Freeze-Thawed Polyvinyl Alcohol/Andrographolide Hydrogels

Halida Rahmi Luthfianti, William Xaveriano Waresindo, Dhewa Edikresnha, Agus Chahyadi, Tri Suciati, Fatimah Arofiati Noor, and Khairurrijal Khairurrijal*

Cite This: *ACS Omega* 2023, 8, 2915−2930

Read Online

ACCESS | Metrics & More | Article Recommendations

ABSTRACT: Andrographolide (AG) is one of the compounds in *Andrographis paniculata*, which has a high antibacterial activity. This paper reports the freeze−thaw method's use to synthesize polyvinyl alcohol (PVA) hydrogels loaded with AG and its characterization. From the morphological examination, the porosity of the PVA/AG hydrogel was found to increase with the increasing AG concentration. The swelling degree test revealed that the hydrogels' maximum swelling degrees were generally greater than 100%. The composite hydrogel with the highest fraction of andrographolide (PAG-4) showed greater weight loss than the hydrogel without AG (PAG-0). The molecular interaction between PVA and AG resulted in the narrowing of the band attributed to the O−H and C═O stretching bonds and the emergence of an amorphous domain in the composite hydrogels. The loading of AG disrupted the formation of hydroxyl groups in PVA and interrupted the cross-linking between PVA chains, which lead to the decrease of the compression strength and the crystallinity increased with increasing AG. The antibacterial activity of the composite hydrogel increased with increasing AG. The PAG-4 hydrogel had the highest antibacterial activity of 37.9 ± 4.6^{b} %. Therefore, the PVA/AG hydrogel has the potential to be used as an antibacterial device.

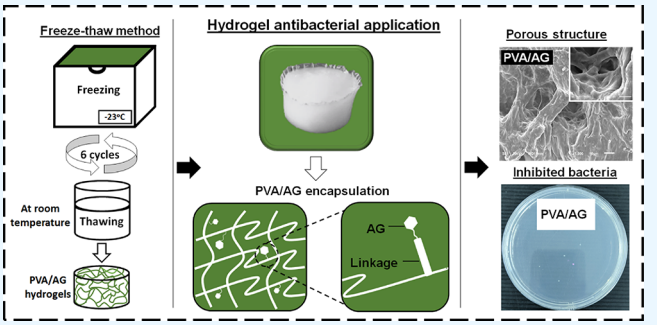

1. INTRODUCTION

Hydrogels are materials composed of polymer chains with three-dimensional cross-linked structures, which can absorb water and are structurally soft and flexible.[1] Hydrogels can be fabricated from natural polymers and synthetic polymers.[2] Polyvinyl alcohol (PVA) is the most widely utilized synthetic polymer due to its good mechanical properties, non-toxicity, pH sensitivity, and biocompatibility.[3] The hydrogels can be synthesized through physical cross-linking (freeze−thaw), chemical cross-linking, and irradiation.[4] In particular, the freeze−thaw method has a competitive advantage compared to others. It is a straightforward process, which produces hydrogels with strong mechanical properties.[5] The freeze−thaw method consists of repeated cycles of freezing and thawing of a polymer−liquid system, forming ice crystals in the polymer precursor solution so that cross-linking between polymer chains occurs.[6] A strong cross-linking of the PVA hydrogel occurs in the microstructure after the fourth cycle,[7] the chestnut starch can be observed as a strong cross-linking hydrogel at three cycles, and the potato and the yam starch are after the first cycle of freezing−thawing.[8]

Currently, hydrogels have been thoroughly developed for wound dressing application. The porous structure of hydrogels makes them capable of maintaining the supply of oxygen hence upholding the moisture level.[9] On the other hand, the hydrophilicity of the polymer causes them to attract water molecules. Therefore making them capable to absorb wound exudate.[10] By loading bioactive compounds into the hydrogels, the composite hydrogels can further accelerate the wound healing process and prevent wound infection.[11] While the stability of the compounds is also increased, which means that the compounds are not easily degraded, as there will be molecular interaction between the compounds and the matrix.[12]

To realize diverse antibacterial composite hydrogels for wound dressing application, several researchers have recently reported PVA hydrogels loaded with various bioactive compounds. Examples of composite PVA hydrogels are the PVA hydrogel loaded with diphlorethohydroxycarmalol (DPHC) isolated from brown alga *Ishige okamurae* as an antimicrobial agent.[13] The addition of DPHC resulted in an

Received: August 9, 2022
Accepted: November 23, 2022
Published: January 9, 2023

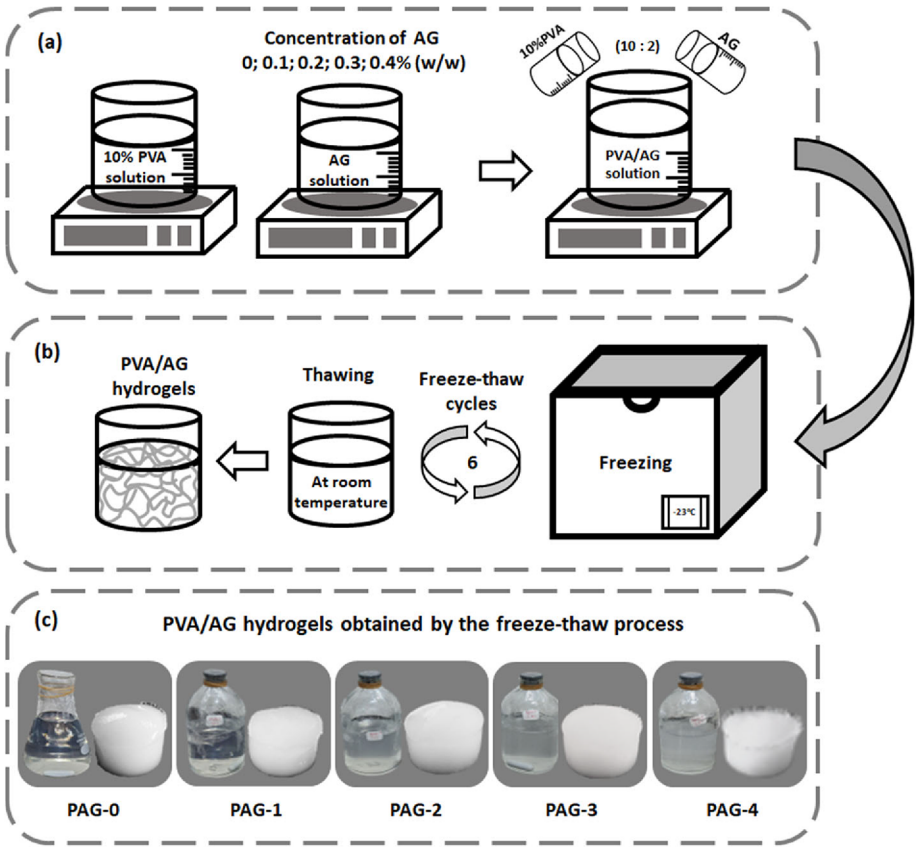

Figure 1. Schematic of the fabrication of hydrogels: (a) preparation of PVA/AG precursor solution, (b) freeze−thaw process, (c) and PVA/AG hydrogels obtained by the freeze−thaw process.

increased porous structure and an antibacterial activity against *S. aureus* and *P. aeruginosa* by 99% after 360 min. In another study, the PVA hydrogel was loaded with a red betel extract with a mixture of ethanol and water as the solvent system.[14] The maximum antibacterial activities were found to be 16.79 ± 2.61 and 24.10 ± 8.94% g^{-1} against *P. aeruginosa* and *S. aureus*, respectively.[15] The antibacterial activity of composite hydrogel loaded with plant extracts was also demonstrated by Waresindo et al. in their research. The antibacterial activities of the PVA/guava leaf extract hydrogel were up to 15.79 ± 0.29 and 17.93 ± 0.78% g^{-1} against *P. aeruginosa* and *S. aureus*, respectively.[15] When the PVA hydrogel was loaded with an *Ipomoea pes-caprae* extract then-synthesized using an electrospinning method, a significantly higher cumulative release than the conventional hydrogel at 2 and 4 h was observed due to the highly porous structure of the electrospun hydrogel.[16] The use of electrospinning in a previous study was able to produce PVP nanofibers loaded with a *Chromolaena odorata* extract with antibacterial potential, but the insignificant mass of nanofiber results in a zone of inhibition hard to observe.[17] On the other hand, the electrospun hydrogel with an inhibition zone diameter of 3.37 ± 0.15 cm showed favorable antibacterial activity against *S. aureus*.[16] In another research, a PVA hydrogel composite with silver nanoparticles and acacia gum (polysaccharide) has been synthesized using the gamma radiation method.[18] The effect of adding acacia gum was the following: the antibacterial activity against Gram-negative bacteria was decreased, the degree of swelling of the hydrogel was increased, and a biocompatibility material was obtained.

Andrographolide (AG) is one of bioactive compounds proven to possess antibacterial activity and a variety of pharmacological activities such as anti-inflammatory, anti-diabetes, and anticancer.[19] Hence, it has been applied as an ingredient in a traditional medicine, also called *jamu*, in Indonesia.[20] AG can be isolated from the herb *Andrographis paniculata* (Burm.f). Ex. Nees. with the concentration percentage around 2.67−5.94% (w/w) and an average of 4.186%.[21] However, the antibacterial effectiveness of AG alone is still under research. In previous research, AG was found to have antibacterial activity against Gram-positive bacteria, vancomycin-resistant *Enterococcus*, and methicillin-resistant *Staphylococcus aureus*, while it was shown to possess considerable antibacterial activity against Gram-negative *Escherichia coli*.[22] In another report, it is stated that AG combined with azithromycin inhibited the in vitro formation of *Pseudomonas aeruginosa* biofilm, hence opening a path for a new combination for antibacterial treatment.[23] Additionally, AG and its synthetic equivalents are reported to have good antibacterial activity both in vitro and in vivo. Specifically, AG can hinder the growth of bacterial biofilms, inhibit the virulence factors, separate the adhesion between bacteria, and destroy the bacterial integrity in direct bacteriostatic action.[24]

Nevertheless, the clinical application of AG is still difficult due to its poor solubility. Hence, there is a thorough effort to increase the clinical effectiveness of AG by modifying the structure to increase the solubility or by improving the delivery system.[25] To the best of our knowledge, the loading of AG into PVA hydrogels (PVA/AG hydrogels) has never been studied. In this paper, we report the study on the effect of varying AG

https://doi.org/10.1021/acsomega.2c05110
ACS Omega 2023, 8, 2915−2930

concentration on the physicochemical characteristics and antibacterial activities of the freeze-thawed PVA/AG hydrogels. The physicochemical characterizations included porosity, degree of swelling, mechanical properties, thermal properties, crystallinity, and functional groups. The antibacterial activities were tested by using *Staphylococcus aureus* and *Pseudomonas aeruginosa*.

2. RESEARCH METHOD

2.1. Materials. Polyvinyl alcohol (PVA) powder with a molecular weight of 89,000−98,000 g/mol and 99+% hydrolyzed was purchased from Sigma-Aldrich. Andrographolide (AG) powder was obtained from MarkHerb (Bandung, Indonesia). Ethanol and distilled water were procured from Merck and PT. Brataco, Indonesia, respectively. Phosphate-buffered saline (PBS) solution was brought from the School of Pharmacy, ITB, Indonesia.

2.2. Preparation of PVA/AG Hydrogels. PVA was dissolved in distilled water at a concentration of 10 wt % and stirred using a magnetic stirrer at 96 °C for 3 h to form a clear homogeneous solution. Meanwhile, AG powder cannot be completely dissolved if only using distilled water.[26] Therefore, it is necessary to use an additional liquid to the solvent system to make the AG solution. In this research, we used a solvent system consisting of a mixture of distilled water and ethanol at a weight ratio of 2:1 with the AG concentration at 0 wt % (PAG-0), 0.1 wt % (PAG-1), 0.2 wt % (PAG-2), 0.3 wt % (PAG-3), and 0.4 wt % (PAG-4) and stirred using a magnetic stirrer at room temperature to form homogeneous AG solutions. Subsequently, the PVA and AG solutions were mixed (PVA/AG) at a weight ratio 10:2 at room temperature until a homogeneous solution was obtained. These PVA/AG precursor solutions were then placed in a freezer at a temperature of −23 °C for 20 h (freezing) and then stored at room temperature for 4 h (thawing). This freeze−thaw process was repeated six times to obtain PVA/AG hydrogels. All the processes are schematically shown in Figure 1.

2.3. Physicochemical Characterizations of PVA/AG Hydrogels. Structural morphologies of PVA/AG hydrogels were determined by a scanning electron microscope (SEM) (JEOL, JSM-6510LA). For the investigation, the PVA/AG hydrogels were lyophilized with freeze-drying apparatus (Eyela, FD-5N) to achieve dried hydrogels. They were then cut along their transverse direction.[14] The internal morphology of the freeze-dried PVA/AG hydrogels was observed at magnifications of 1000× and 5000×. The pore size of PVA/AG hydrogels was examined by using ImageJ software (version 64-bit Java 1.8.0_172, NIH, USA). By determining the surface area on the SEM images, we confirmed the pore size[13] of the PVA/AG hydrogel structure.

The swelling degree of the freeze-dried PVA/AG hydrogel was obtained as follows. The hydrogel was dried in the oven at 50 °C for 5 days. The dried hydrogel that was used with previous experiment[14] was then weighed (W_d) and then immersed in the PBS solution at the physiological pH of 7.4 at 37 °C. The weights of the hydrated hydrogel (W_s) were then measured at 0, 3, 6, 12, 24, and 48 h after immersion. The swelling degree of the hydrogel can then be determined from eq 1:

$$\text{degree of swelling (\%)} = \left[\frac{(W_s - W_d)}{W_d}\right] \times 100\% \quad (1)$$

The degree of swelling is important in wound dressing applications, for example, to protect the moisture of the wound area, to predict the absorption capability of wound exudate, and to support the hemostatic process in the wound healing process.[27]

To determine the weight loss of the freeze-dried PVA/AG hydrogel, the following steps were taken. The hydrogels were first dried in an oven at 50 °C for 5 days. The weight of the dried hydrogels was then measured (W_0). The dried hydrogels were then immersed in the PBS solution at 37 °C for 48 h and subsequently dried in an oven at 50 °C for 5 days to remove water content. The hydrogel was weighed again after immersion and drying (W_f). The number of gels remaining indicates the number of cross-links formed on the hydrogel. The weight loss is determined from eq 2

$$\text{weight loss (\%)} = \left[\frac{(W_0 - W_f)}{W_0}\right] \times 100\% \quad (2)$$

Since the biodegradability is an important property of the ideal wound dressing material,[28] the weight loss of the hydrogel after the swelling test must be measured. The weight loss experiment confirmed the degradability or capability of the hydrogel to sustain its form. It is used to investigate the percentage of cross-linking occurring during the freeze−thaw process.

A Fourier transform infrared (FTIR) spectrometer (Bruker, Alpha) with the wavenumber range of 500−4000 cm^{-1} was employed to identify the functional groups and the interactions in the PVA/AG hydrogels. To determine the functional group changes in the hydrogels, the FTIR spectra of the hydrogels were examined.

An X-ray diffractometer (XRD) (Rigaku, SmartLab) was used to characterize the crystallinity of the PVA/AG hydrogels. The X-ray source used Cu Kα radiation that is generated at a voltage of 40 kV and current of 30 mA with the wavelength of 1.5405 Å while the diffraction angle (2θ) was observed from 10 to 90°.

The material testing machine (Sinowon, Universal Material Testing Machine SM-200) was utilized to determine the mechanical strength, including compressive modulus and compressive strength of the PVA/AG hydrogels. The compression modulus was calculated by the slope of the linear stress−strain curve.[29]

A thermogravimetric/differential scanning calorimetry (TG/DSC) apparatus (Hitachi, STA7200) was used for characterizing the thermal properties of the PVA/AG hydrogels. The hydrogel weight was accurately measured while the temperature was increased from 30 to 600 °C at a heating rate of 10 °C/min. The obtained TG/DSC curve was used to determine the melting temperature, residue, and weight loss as the temperature increased. The enthalpy change (ΔH) was calculated from the area below the melting point and then analyzed using Origin 8.5.1 software. The change in enthalpy of PVA (ΔH_{PVA}) was affected by the area below the melting point (ΔH) and the mass fraction of PVA in each sample, as shown in eq 3a. After that, the degree of crystallinity was calculated using eq 3b:[30]

$$\Delta H_{PVA} = \left(\frac{\text{PVA powder (g)}}{\text{total powder (g)}}\right) \times \Delta H \quad (3a)$$

https://doi.org/10.1021/acsomega.2c05110
ACS Omega 2023, 8, 2915−2930

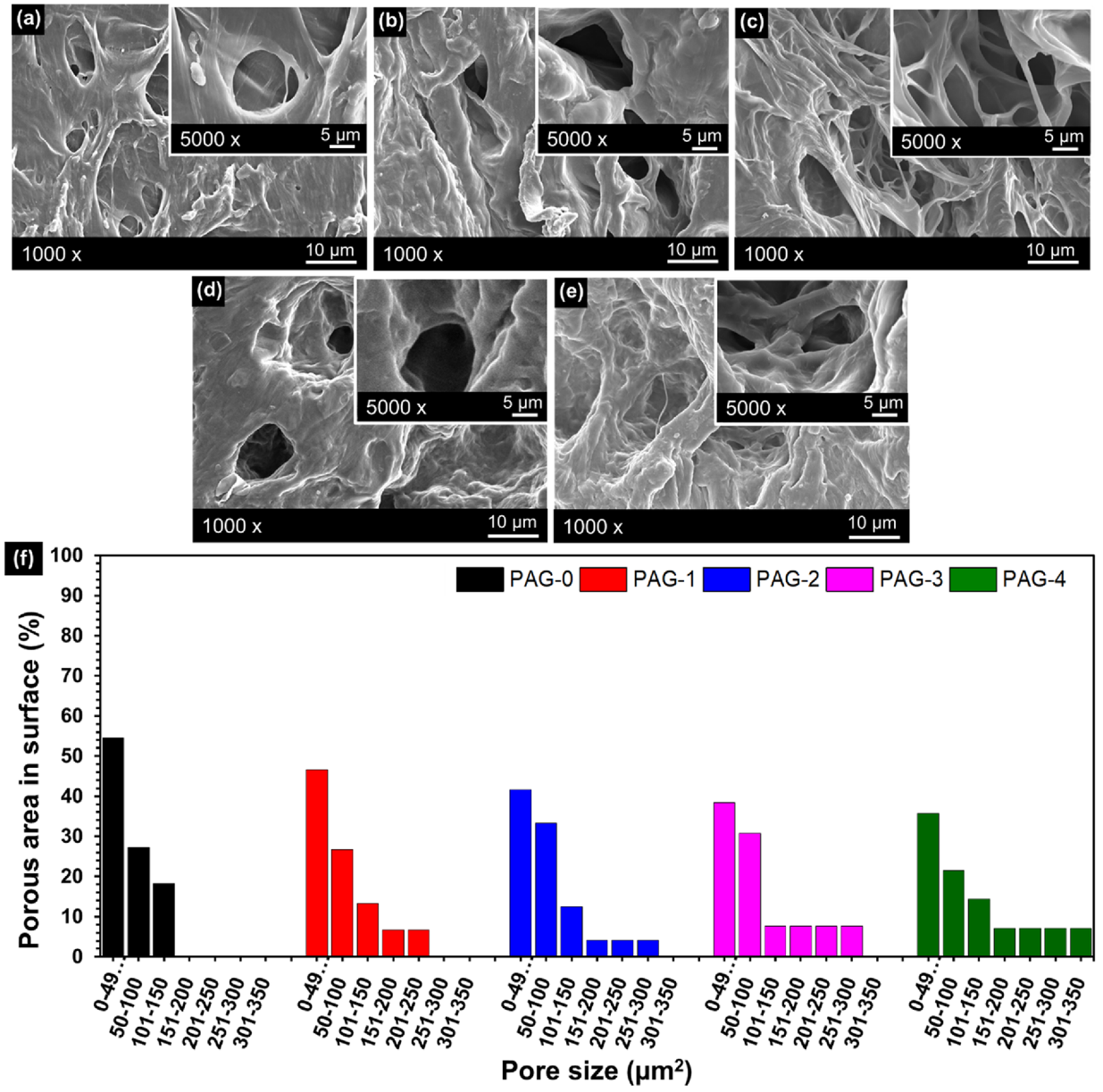

Figure 2. SEM images of the (a) PAG-0, (b) PAG-1, (c) PAG-2, (d) PAG-3, and (e) PAG-4 hydrogels and (f) pore size of PVA/AG hydrogels.

$$\text{degree of crystallinity (\%)} = \left(\frac{\Delta H_{\text{PVA}}}{\Delta H_0}\right) \times 100\% \quad (3b)$$

where ΔH is the enthalpy for melting PVA powder (J/g) and ΔH_0 is the enthalpy of fully crystallized PVA powder (138.60 J/g).[31]

2.4. Antibacterial Test. To calculate the ability of the hydrogel to inhibit bacterial activity, an antibacterial test was performed. Antibacterial activity was tested using the total plate count (TPC) method. The bacteria used were Gram-positive and negative, namely, *Staphylococcus aureus* (ATCC 6538) and *Pseudomonas aeruginosa* (ATCC 9027), respectively. The discs of the PVA/AG hydrogel, in which each of them had 20 mm in diameter, 5 mm in height, and a weight of approximately 1.79 g, were placed on top of the solid Muller–Hinton agar (MHA) on petri dishes. Then, an inoculum of *Staphylococcus aureus* (1.3×10^6 cfu mL^{-1}) or *Pseudomonas aeruginosa* (4.5×10^5 cfu mL^{-1}) was poured onto each hydrogel in a separate container.

Subsequently, the bacteria-poured hydrogels were placed in an incubator at 37 °C for 24 h. The bacteria-incubated hydrogel would show a zone of inhibition, a clear zone indicating the diameter of bacterial inhibition, around the disc. The diameter of inhibition was measured using a micrometer. Next, about 10 μL of solid MHA sample was taken at the edge of the hydrogel and diluted in 100 μL of sodium chloride solution. One milliliter of diluted suspension was dropped on solid MHA in Petri dishes and then incubated at 37 °C for 24 h to determine the spread of bacteria. Bacterial colonies were counted from the dilution to determine the antibacterial activity, which is determined through[32] the equation

https://doi.org/10.1021/acsomega.2c05110
ACS Omega 2023, 8, 2915−2930

$$\text{antibacterial activity} = \frac{[(\log \text{control}(\text{cfu mL}^{-1}) - (\log \text{fibers}(\text{cfu mL}^{-1})]}{\text{mass hydrogel (g)} \times \log \text{control (cfu/mL)}} \quad (4)$$

2.5. Statistical Analysis. The calculations of the various treatments in this experiment were performed in triplicate, and the results were then shown as mean ± standard deviation (SD) followed by ANOVA (analysis of variance) and Tukey's HSD (honestly significant difference) statistical tests.[15] The IBM SPSS 24 software (IBM, USA) was employed to determine a significant difference with the confidence level higher than 95% ($p < 0.05$). Values with various superscript letters differed considerably ($p < 0.05$), whereas those with identical superscript letters did not change significantly ($p > 0.05$).

3. RESULTS AND DISCUSSION

3.1. Morphological Analysis of PVA/AG Hydrogels. Figure 1 shows the synthesis process of PVA/AG hydrogels. All the PVA/AG hydrogels in Figure 1c were opaque with a dense white color. Increasing the PVA content in the hydrogel generally increases the opacity of the hydrogel and thereby reduces light transmission due to the presence of crystalline regions.[33] During the freeze−thaw process, the PVA macromolecules undergo densification by means of ice crystal formation during freezing while becoming orderly structured during thawing.[34] The cross-linking between polymer chains is accompanied by the formation of ice crystals; hence, a larger amount of cross-linking can be formed by either increasing the freeze−thaw cycles.[35] In this experiment, dense white hydrogels were obtained after the freeze−thaw process with six cycles, similar to previous studies.[7]

SEM images of the cross-sectional view of the freeze-dried PVA/AG hydrogels are presented in Figure 2. The PAG-0 hydrogel (pure PVA) does not show any phase separation between the liquid and the solid phase. For the precursor solution, the PAG-0 hydrogel used only distilled water as the solvent, resulting in a complete evaporation of the water fraction during the freeze−dry process and hence causing the bulk of the PVA hydrogel samples to collapse.[36] Meanwhile, the PAG-1 to PAG-4 hydrogels (Figure 2b−e) show the phase separation between the liquid and the solid phase, where the liquid phase becomes the pores. Phase separation can be observed due to the presence of ethanol, which does not completely evaporate during the freeze-drying process; also ethanol prevents the hydrogel from collapsing.[14] The formation of pores occurred as follows: during the freezing process, ice crystals grew along the temperature gradient. Within the solution phase, there were many segregated PVA chains where the hydroxyl groups of the PVA chains form an intermolecular hydrogen bonding between them.[37] The existence of AG bioactive compound interfered with the bonding process between the hydroxyl groups and also with the formation of crystallinities, resulting in pores inside the bioactive compound−composited hydrogel.[7,13]

The pore size of the PVA/AG hydrogels is shown in Figure 1f. It was found that PAG-0 had a more regular porous structure than the composite hydrogels (PAG-1 to PAG-4). The pore size of PAG-0 hydrogel was within the range of 0−49 μm^2 (55%), 50−101 μm^2 (27%), and 101−150 μm^2 (18%), while the PAG-4 hydrogel shows various pore sizes and large pore size was within the range 0−49 μm^2 (36%), 50−101 μm^2 (21%), 101−150 um^2 (14%), 151−200 μm^2 (7%), 201−250 μm^2 (7%), 251−300 μm^2 (7%), and 301−350 μm^2 (7%). The enlarged and irregular pore size was caused by AG, which interfered with the formation of hydroxyl groups in PVA during the freeze−thaw process.[13,38] The structure and pore size of the hydrogel also affect the controlled release of the antibacterial compounds. According to Zou et al., the hydrogel, which has a porous morphological structure and large pore size, has excellent antibacterial activity against *S. aureus* and *E. coli* bacteria.[39] The porous structure of a wound dressing can provide a space for the encapsulation of active substances as well as cell growth and proliferation. In addition, the porous structure is also useful in the absorption of the wound exudate and as a space for oxygen supply to the closed cells. Thus, hydrogels with high porosity can help accelerate the wound healing process and have more effective antibacterial activity.[40] Based on this fact, PAG-4 with the largest pore size is estimated to show the highest antibacterial activity, which will be proven in the antibacterial test.

3.2. Degree of Swelling and Weight Loss. Figure 3a depicts the swelling degree of the obtained PVA/AG hydrogels. It is shown that all the hydrogels had significant absorptive capabilities for the first 24 h. Afterward, the swelling degree was relatively constant up to 48 h, indicating that the equilibrium condition had been reached.[13] Due to the polymer chains relaxing, the hydrogel network stretched as a result of

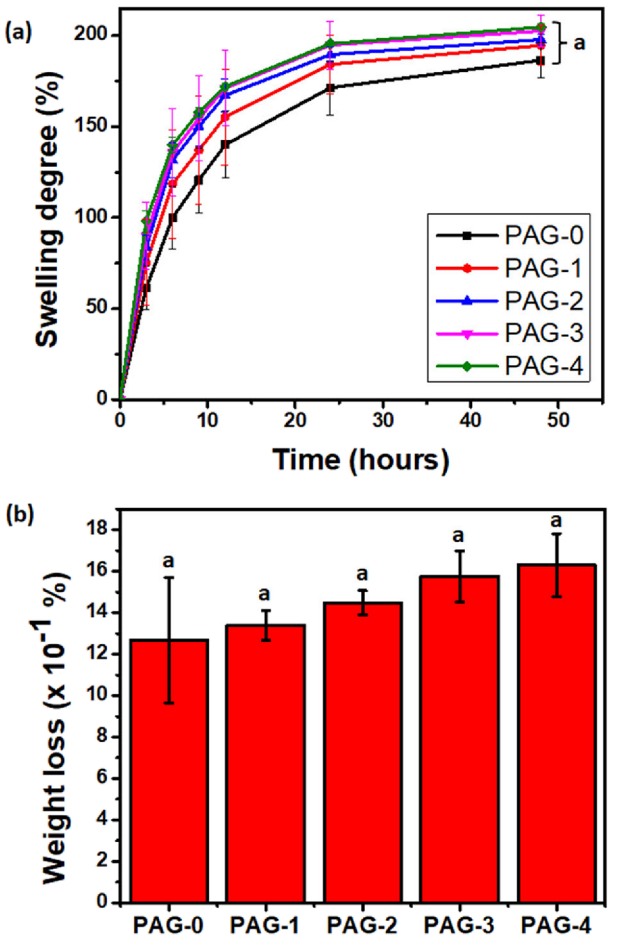

Figure 3. (a) Swelling degrees of PVA/AG hydrogels and (b) weight losses of PVA/AG hydrogels.

https://doi.org/10.1021/acsomega.2c05110
ACS Omega 2023, 8, 2915−2930

PBS molecules entering it.[41] Moreover, the addition of the AG fraction resulted in the increased swelling degree of the hydrogel. Since the AG interfered with the hydrogen bonds in PVA, a higher AG content consequently led to a lower cross-linking density and chain entanglement.[37] The lower cross-linking density allows the PBS solution to penetrate the hydrogel and increase the swelling degree.[42] Additionally, a lower AG fraction corresponded to a higher PVA content, which then led to a lower porosity. With a smaller pore size, the amount of PBS solution that enters the hydrogel structure is also smaller.[43] The hydrogel PAG-0 had the lowest swelling degree after 48 h, at 186.5 ± 9.7[a] % of the original weight, since it had the smallest porosity. Figure 3a also shows that the swelling degree of the hydrogels increased with the increasing fraction of AG bioactive compound. Their values were 194.5 ± 11.0[a], 197.8 ± 3.1[a], 202.5 ± 9.0[a], and 204.7 ± 1.7[a] % for the hydrogels PAG-1, PAG-2, PAG-3, and PAG-4, respectively. Therefore, the results match the previous research. There was no significant difference between the groups ($p > 0.05$).

Figure 3b illustrates the increase in weight loss as the AG bioactive compound content increases. The hydrogel weight loss describes the strength of the hydrogel structure in maintaining its shape. In other words, the hydrogel weight loss shows the remaining gel fraction after being dissolved in PBS.[15] The hydrogel PAG-0 had the lowest weight loss at 1.26 ± 0.30[a] %. Thus, hydrogel PAG-0 had the strongest ability to maintain its structure. The increase of AG fraction reduced the structural strength of the PVA/AG hydrogel. The hydrogel PAG-4 with the highest weight loss at 1.63% ± 0.15%[a] therefore had the weakest structure. The weight loss of PAG-0 was caused by the dissolution of PVA only, while the loss of the composite hydrogel (PAG-2 to PAG-4) involved the release of bioactive compounds into the PBS solution. During the swelling degree test, the polymer chains expanded due to the PBS solution entering the hydrogel network during the swelling process, hence allowing the bioactive compound to leave the hydrogel network.[14] Therefore, the weight loss of the bioactive compound affected the degree of swelling of the hydrogel sample. The weight loss between groups did not show a significant difference ($p > 0.05$).

3.3. FTIR Spectra. Figure 4 demonstrates FTIR spectra of the PVA powder, AG powder, and PVA/AG hydrogels, and their observed characteristic peaks are tabulated in Table 1. The FTIR spectrum of PVA powder had a broadening peak located around 3000−3664 cm^{-1}, indicating the O−H stretching of the hydroxyl (O−H) group, while the peak at 2938 cm^{-1} is attributed to the stretching of C−H.[44] Other peaks of the PVA powder are 1656 and 1442 cm^{-1}, which are assigned to the C═O stretching[45] and C−H bending vibration,[46] respectively. Also the peaks at 1144 and 1097 cm^{-1} are attributed to C−O stretching.[47]

Moreover, the peak at 1144 cm^{-1} is due to the C−O stretching vibration, which is related to its crystallinity.[47] The appearance of this peak confirms the semicrystalline nature of PVA powder, as also confirmed by its respective XRD spectra that will be discussed later. The FTIR spectrum of AG powder has also a broad peak around 3030−3668 cm^{-1}, which is similar to that of PVA powder, indicating the presence of O−H stretching of the hydroxyl group, and two peaks at 2928 and 2847 cm^{-1}, denoting the existence of C−H stretching.

Other peaks contributed by the carboxylate ester compound of AG are as follows: (i) those at 1726 and 1673 cm^{-1} represent the stretching of the carbonyl (C═O) group and

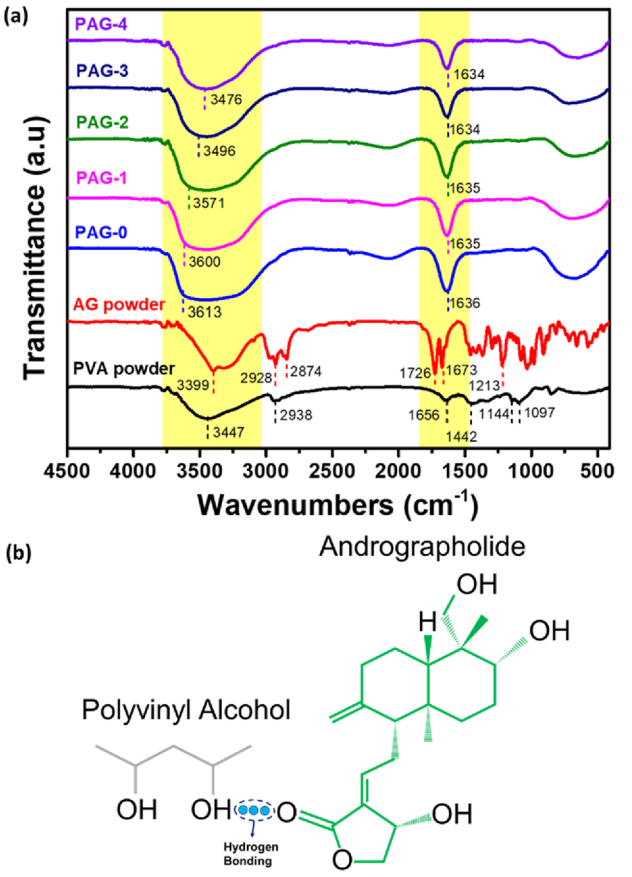

Figure 4. (a) FTIR spectra of PVA powder, AG powder, and PVA/AG hydrogels and (b) hydrogen bond between PVA and andrographolide.

(ii) that at 1213 cm^{-1} represents the C−O stretching vibration. All these observed peaks are in agreement with the previous reports.[48,49]

We observed three distinct features between the PVA powder spectrum with its hydrogel form (PAG-0) due to intermolecular cross-linking during the freeze−thaw process: (i) the widening and shifting of wavenumber attributed to the hydroxyl group (O−H stretching vibration) from 3000−3664 to 3000−3702 cm^{-1} due to the cross-linking of O−H chains during hydrogel synthesis,[50] (ii) the vanishing of the stretching and bending vibration of C−H peaks (2938 and 1442 cm^{-1}) due to the formation of rigid molecules,[51] and (iii) the disappearance of C−O stretching due to the amorphous nature of the hydrogel form.[47]

Additionally, the peaks of the AG hydrogel exist at the FTIR spectra of the composite hydrogels. In previous research, the type of intermolecular bonding between the extract and the polymer matrix was mostly found in the form of hydrogen bonds (O−H groups)[12], as illustrated in Figure 4b. Some examples are the nanofiber and nanoparticle matrix loaded with a mangosteen peel extract[52] and a turmeric extract[53] and the hydrogel matrix loaded with a *Piper crocatum* extract[14] and a guava leaf extract.[15]

Table 1 demonstrates the peaks of composite hydrogels (PAG-1 to PAG-4), which shows the peak changes in the hydroxyl group and carboxyl group. The peaks from O−H stretching vibration were at 3613, 3600, 3571, and 3496 cm^{-1} for PAG-1, PAG-2, PAG-3, and PAG-4, respectively. Meanwhile, the peak wavenumbers for the composite hydrogel

https://doi.org/10.1021/acsomega.2c05110
ACS Omega 2023, 8, 2915−2930

Table 1. Wavenumbers and Functional Groups of PVA Powder, AG Powder, and PVA/AG Hydrogels

PVA	AG	PAG-0	PAG-1	PAG-2	PAG-3	PAG-4	vibrational mode
3447	3399	3616	3600	3571	3496	3476	O−H stretch[54]
2938	2928; 2847						C−H stretch[44,46]
1656	1726; 1674	1636	1635	1635	1634	1634	C═O stretch[45,46]
1442							C−H bend[44]
1144;1097	1213						C−O stretch[47]

(PAG-1 to PAG-4) attributed to C═O stretching appeared at 1636, 1635, 1635, and 1634 cm^{-1}, respectively. The increase in the AG fraction in the composite hydrogel caused the wavenumber associated with O−H stretching and C═O stretching to be shifted to smaller wavenumbers with narrower peaks.

3.4. X-ray Diffraction Patterns. Figure 5 depicts the XRD patterns of the PVA powder, AG powder, and PVA/AG hydrogels. The PVA powder has two halos with peaks at 2θ values of 19.66° and 40.87°, indicating the semicrystalline properties.[6] The crystallinity was determined by the ratio of the strongest area over the total area of the peaks.[14] The degree of crystallinity of PVA powder of about 55%, which shows slightly lower than in previous studies.[14] Additionally, the AG powder exhibits sharp peaks at 2θ values of 12.12, 14.86, 15.8, 17.56, 22.72, and 26.8°, which indicate the crystal phase with a degree of crystallinity of about 91%.

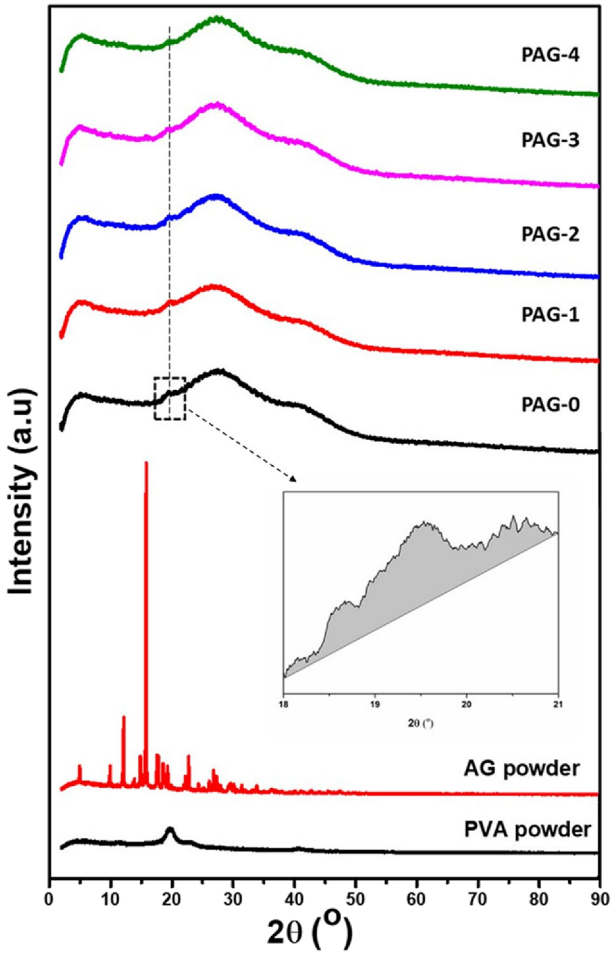

Figure 5. XRD patterns of PVA powder, AG powder, and PVA/AG hydrogels.

The XRD patterns of the PVA/AG hydrogels show two broad halos at 2θ of about 27° and 42°, implying that they are amorphous. The characteristic peaks of the AG powder disappear in the XRD pattern of the PVA/AG hydrogel, which indicates that the AG has been fully transformed to be amorphous inside the matrix.[55] During the hydrogel formation in the freeze−thaw process, the PVA chains become disoriented and no longer arranged as lamellar. The process also causes the formation of a hydrogel network consisting of knots and porous walls.[14] These knots are also known as the crystal domain of the hydrogel, which provides dimensional stability of the hydrogel. However, the increase of AG content in the hydrogel (PAG-0 to PAG-4) resulted in the decrease of the crystal domain, as indicated by the degrees of crystallinity of 2.53, 1.65, 0.89, 0.61, and 0.45%, respectively. The degree of crystallinity of the hydrogel was analyzed with a ratio of a small area (18 to 21°) over the total area of the peaks, which indicates a small PVA content. During the freeze−thaw process, AG interfered with crystallite formation of PVA, which caused most parts inside the hydrogel to be porous; hence, the structure was amorphous.[13,14] The amorphous structure of the hydrogel shows widened XRD peaks with the addition of AG content. In the XRD pattern of all PVA/AG hydrogels (PAG-0 to PAG-4), the amorphous broad halo peak at 19.66° shifts to a 2θ of 27°, which proves the existing molecular interaction between the bioactive compound (AG), water, ethanol, and the PVA chains.[14,15,52]

An amorphous matrix can dissolve easily and is soluble. When a bioactive compound or drug was loaded in an amorphous matrix, the dissolution rate can be high and the loaded drug can be released into the surroundings more easily[53] In the case of the crystal structure, a certain amount of energy is needed to break the crystal lattice in order for a drug to be released from a crystal structure or for a crystal structure to dissolve. Such an energy is not needed to break down the amorphous structure and release the bioactive component from it. Hence, the amorphous phase in the PVA/AG hydrogel is advantageous for antibacterial applications, in which the AG can be released easily. Additionally, the presence of molecular interactions between compounds and the hydrogel matrix serves to increase the stability of bioactive compounds so that the compounds are not easily degraded.[12]

3.5. Mechanical Properties. Figure 6 demonstrates the stress versus strain curves, which show a similar characteristic with the previous research.[56] The curves of the composite hydrogels PAG-0 to PAG-4 are exponential, resembling a ″J″ shape, which indicates a high compressive strength at the high strain portion. The average value was reported by taking at least three measurements of each sample. The *R*-squared value of the exponential fitting was more than 0.99. Therefore, it can explain the viscoelastic characteristic of the hydrogels,[57] in which the hydrogels were still not damaged when the strain was about 36%.

https://doi.org/10.1021/acsomega.2c05110
ACS Omega 2023, 8, 2915−2930

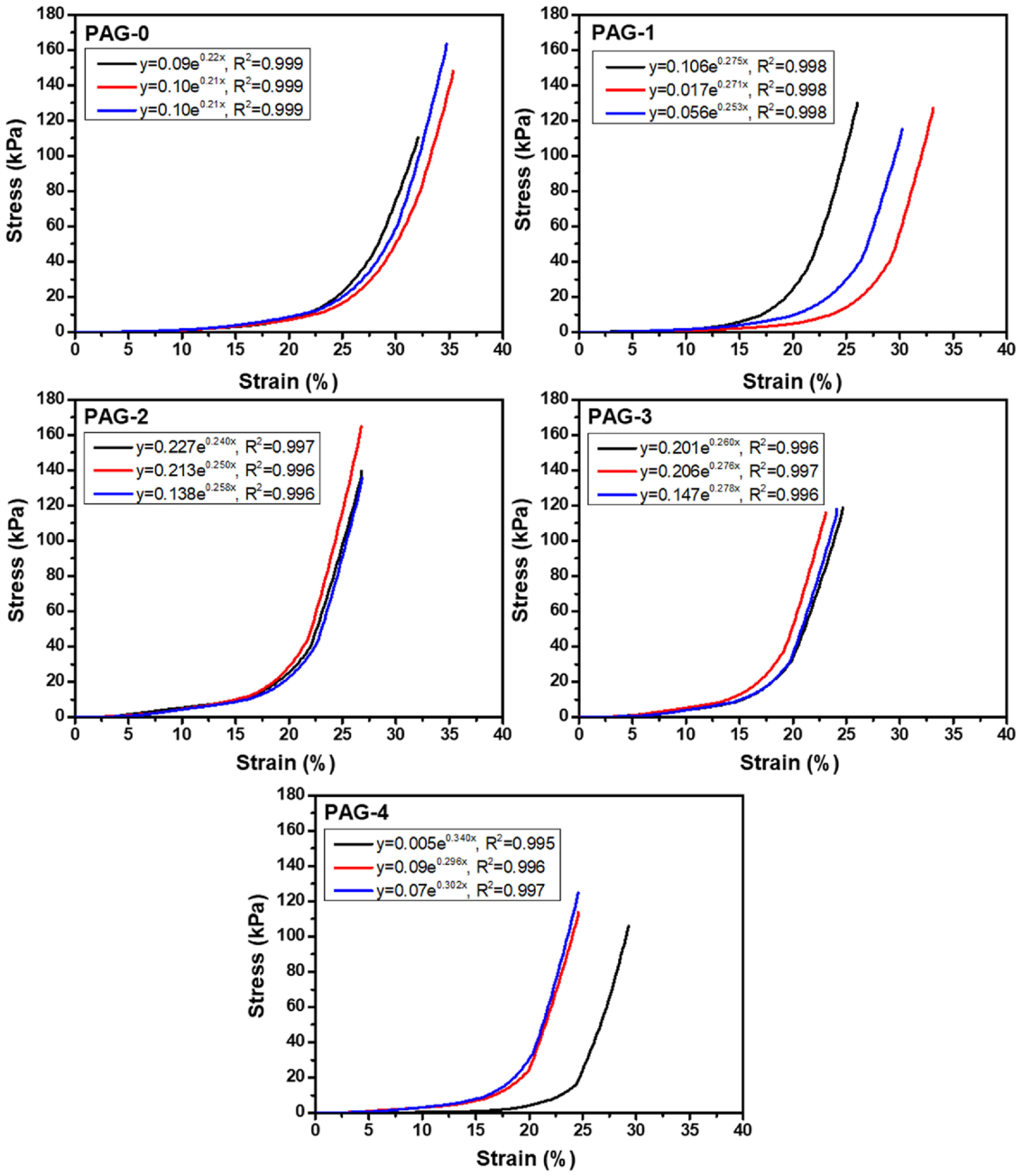

Figure 6. Relationship between stress and strain of PVA/AG hydrogels.

The PVA hydrogel is a three-dimensional network structure, which shows the amorphous structure. The PVA molecular chains allow the hydrogel to be flexible in response to external forces, i.e., by rearranging themselves simultaneously, thus resulting in a relatively high compressive strength, and is beneficial to the viscous characteristics of the hydrogel.[57] The results of this study are in line with previous research.[58]

Table 2 indicates the compressive modulus and the compressive strength of the PVA/AG hydrogels. The compressive modulus was obtained from a mathematical approach,[59] by the derivation of the exponential fitting equation in Figure 6 as the compressive modulus equation:

$$y = ae^{bx}$$
$$y' = E = by \quad (5)$$

Table 2. Compressive Properties of the Hydrogels

sample	compressive modulus (kPa)	compressive strength (kPa)
PAG-0	21.4 ± 0.8[a]	137.2 ± 23.3[a]
PAG-1	26.6 ± 1.2[a]	123.9 ± 3.5[a]
PAG-2	24.9 ± 0.9[a]	122 ± 15.0[a]
PAG-3	27.2 ± 1.0[a]	117.6 ± 1.3[a]
PAG-4	31.3 ± 2.4[a]	113.9 ± 1.2[a]

For the analysis, the compressive modulus was determined on the stress value y = 100 kPa. Hence, the compressive modulus can be found from the multiplication of the rate of growth, b. It was found that the compressive modulus of composite hydrogels tended to increase with the increase of AG fraction since the increase of AG is related to the increase of the ethanol fraction in the PVA/AG composite hydrogel.[14]

https://doi.org/10.1021/acsomega.2c05110
ACS Omega 2023, 8, 2915−2930

During the synthesis process, the ethanol fraction was stored in the hydrogel as a free liquid because it did not freeze at the freezing point of −23 °C. The presence of the ethanol fraction as a free liquid in the hydrogel causes the hydrogel composite to become soft.[58]

The mean compressive strength was obtained from the average of the maximum stress for the repeated measurements of each sample. The high compressive strength corresponds to a higher cross-linking density of the hydrogels. The cross-linking density is influenced by the number of freeze−thaw cycles and the duration of freezing.[60] In this study, the number of cycles was six with the duration of freezing being 20 h and the duration of thawing being 4 h. The PAG-0 hydrogel had the highest compressive strength at around 137.2 ± 23.3[a] kPa. The compressive strength of the composite hydrogels of samples PAG-1 to PAG-4 decreased with the increase of AG concentration since the presence of AG led to a decrease in cross-linking density.[61] Meanwhile, the decrease of the cross-linking density can be indicated by the increase of the porosities of the hydrogels.[13] It has previously been proven by SEM images that the porous area on the cross-sectional view of the hydrogel increased with increasing AG concentration. During the crystallite formation of PVA, AG had interfered in the cross-linking process between hydroxyl groups and decreased the cross-linking density of the PVA/AG composite hydrogel.[37,38] In general, the physical properties of the hydrogel loaded with AG show insignificant differences between groups ($p > 0.05$) since the AG content is only slightly increased from PAG-0 to PAG-4 (0.012 to 0.048 g).

Wang *et al.* in their publications reported the results of the test animal skin compression test as follows: at a strain level of 25%, the skin of mice showed a maximum stress of 31.78 kPa, while that of pig skin showed 39.97 kPa. From these results, they concluded that mammalian skin basically has the same characteristics.[62] In the current study, the maximum stress of all samples at a strain level of 25% shows a value above 100 kPa. In addition, other studies have concluded that human skin tissue has a compression modulus ranging from 1 to 100 kPa.[63,64] Therefore, the PAG-0 to PAG-4 samples in this study met the criteria as wound dressing materials with a maximum stress above 100 kPa and compression modulus in the range of 1 to 100 kPa.

3.6. Thermal Properties. The thermal behavior was examined by DSC and TGA. The DSC test was carried out to analyze the intermolecular interactions between the media delivery and the bioactive compound (drug), which are not independent of each other. The TGA test can be used to determine the stability of a bioactive in the range of room temperature to body temperature.[52] In the pharmaceutical field, thermal characterization has been utilized to analyze pharmaceutical stability in the studies of bioactive excipient compatibility.[65] Meanwhile, DSC and TGA assays are conducted for the development and research of pure drug compounds to investigate the stability of novel drug compounds and to investigate polymorphic and purity forms of the drugs.[66] The study on the thermal behavior is usually done as an additional characterization in the development of drug delivery media, for example, hydrogels,[14,15] nanoparticles,[55] and nanofibers.[52,67] In another research, the DSC test on a hydrogel containing red betel leaf extracts showed a phase transition of the extract from crystalline to an amorphous structure after being encapsulated in a hydrogel.[14] A hydrogel with guava leaf extracts also causes a change in the melting point of the PVA hydrogel to a lower temperature.[15]

Figure 7 shows the DSC graph of PVA powder, AG powder, and PVA/AG hydrogels. The thermogram of the PVA powder shows endothermic peaks at 221, 256, and 440 °C. According to ref 55, the melting point of PVA is at 230 °C.[31] The difference between the experiment's results and the reference indicates the existence of impurities in the PVA powder. The

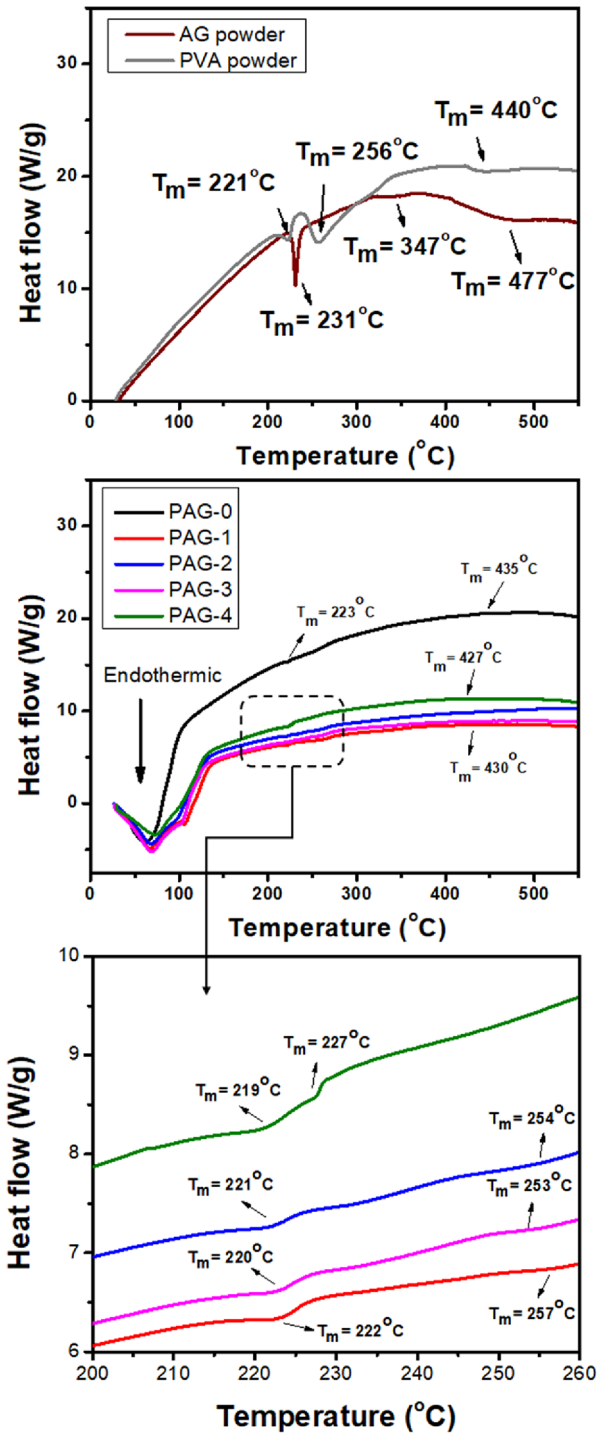

Figure 7. DSC thermograms of AG powder, PVA powder, and PVA/AG hydrogels.

https://doi.org/10.1021/acsomega.2c05110
ACS Omega 2023, 8, 2915−2930

impurities widened the endothermic peak and changed the melting point.[55]

The area of the endothermic peak around 221 °C was used to calculate the change in enthalpy of PVA powder because that temperature is closer to the melting point of the reference than any other. In contrast, the presence of a broad endothermic peak at 256 °C is associated with removing of the hydroxyl group.[14] The change of enthalpy at 221 °C was found to be at about 53.4 J g^{-1}. All PVA/AG hydrogel samples (PAG-0 to PAG-4) had significant endothermic (melting) peaks below 150 °C, indicating the water evaporation from the hydrogel samples in which the weight reduction was more than 80% for all hydrogels.[15]

As presented in Table 3, the change of enthalpy decreases as the PVA fraction decreases. Since the change of enthalpy corresponds to higher thermal stability,[68] the hydrogel with the larger PVA fraction had a higher thermal stability. The change of enthalpy for all samples was below the enthalpy change required to melt fully crystallized PVA, which is 138.60 J g^{-1}[31]. By using eq 3, the degree of crystallinity of the PVA powder was found to be 38.5%, while that determined using XRD data was 55%. The difference of degrees of crystallinity of PVA obtained by DSC and XRD were also shown by several previous studies.[14,69] The difference can be explained as follows: when using DSC, the degree of crystallinity is contributed by the crystal content of PVA in the dry state, while using XRD, it is from the crystal content of the hydrogel in the hydrated state in which scattering of water and ethanol has an important effect. The degree of crystallinity based eq 3 is usually used for semicrystalline polymers where there is a clear distinction between the crystalline and amorphous regions.[70] Crystallized polymers simply consist of aligned polymer chains, forming lamellae.[71,72] According to previous studies, eq 3 was only used to determine the degree of crystallinity of poly(vinylidene fluoride) (PVDF) although it did consist of many other materials.[73,74] In other previous studies, eq 3 has been used to calculate the degree of crystallinity of several composite polymers, i.e., poly(vinylidene fluoride-*co*-hexafluoropropylene) (PVDF-HFP),[75] poly(ethylene oxide)/poly(vinyl pyrrolidone) (PEO/PVP-TiO_2),[76] polyvinyl alcohol (PVA),[14,31] polyethylene-oxide/poly(L-lactide) (PEO/PLLA),[77] and polyetheretherketone (PEEK).[78] Additionally, the previous research also showed that the degree of crystallinity in DSC was only analyzed for the effect of the polymer (PVA), while the degree of crystallinity of the red betel extract was calculated on the XRD section.[14] For non-polymer materials with various crystal structures, such as AG, the enthalpy of its fully crystallized form was not found in the reference. However, we propose to determine the change of enthalpy of a fully crystallized AG ($\Delta H_{0\ -\ AG}$) from the experimental results of XRD and DSC according to eq 4 taken from a previous report,[79] where ΔH is the change of enthalpy of AG powder (29 J/g).

Table 3. Thermal Properties

sample	ΔH (J/g), during melting of PVA	degree of crystallinity of PVA (%)	residue at 600 °C (%)
PVA powder	53.4	38.5	4.2
AG powder	29.0		1.1
PAG-0	25.9	18.7	1.6
PAG-1	24.9	18.0	1.7
PAG-2	23.5	17.0	1.9
PAG-3	22.1	15.9	1.0
PAG-4	18.9	13.7	1.3

$$\Delta H_{0-AG} = \left(\frac{100\%}{\text{degree of crystallinity AG in XRD}}\right) \times \Delta H \quad (4a)$$

The enthalpy of fully crystallized AG that we obtained from experiments and eq 4 was about 31.87 J/g.

The degrees of crystallinity for PAG-0 to PAG-4 was 18.7, 18.0, 17.0, 15.9, and 13.7%, respectively. The degree of crystallinity was reduced as the PVA fraction decreased because the number of polymer chains decreased, as reported by previous studies.[14] The degree of crystallinity results obtained from DSC was not similar to the XRD results, which show an amorphous structure. The crystallinity of AG and the scattering of liquid (ethanol and water) have an important effect during determination of the degree of crystallinity from XRD, while the calculation of the degree of crystallinity from DSC was not affected by these two factors. During the DSC test, the hydrogels were heated to a temperature of 600 °C, then the water evaporated, and the hydrogel was dried. As for eq 3, the crystallinity of the bioactive compound is not included in the equation. Thus, while the DSC results present the approximate degree of crystallinity of the PVA component in the dried hydrogel, the XRD results show the crystallinity of the hydrogel with an amorphous structure in the hydrated state.[14]

Additionally, the decrease in PVA crystallinity was due to fewer folding polymer chains and the number of overlapping PVA chains showed a reduction.[31] With the PVA content was decreased, the total heat required to melt the sample was reduced while the melting point shifted to a slightly lower value.[14] During the final phase around 371 to 470 °C, the mass was significantly reduced, as will be explained in the discussion of TGA.

Figure 7 shows the curve of the AG powder on the gray line. For AG powder, there are two wide endothermic peaks at temperatures of 231 and 447 °C, which agree with the previous study.[80] By calculating the area under the endothermic peak around the melting temperature, the heat needed to melt the AG was found to be at about 22.2 J/g. The mass decomposition of AG began around this first endothermic peak temperature. Moreover, the moisture loss and evaporation of the volatile components in the bioactive chemicals might have also partially resulted in the endothermic peak around 231 °C[14]; hence, the complete decomposition process occurred at a temperature of about 447 °C.

The decomposition curves of PVA, AG, and the PVA/AG hydrogels as presented in Figure 8 were taken from the thermogravimetric analyzer test. The decomposition of PVA powder occurred in three phases, as reported by previous studies.[81] The first phase was at temperatures below 100 °C, caused by the evaporation of adsorbed water and water bound in the hydrogel network of polymer molecular chains, mainly through hydrogen bonds. In the second phase, there was a significant weight reduction between 211 and 339 °C due to a decrease in hydroxyl groups, producing a conjugated structure. Lastly, the carbonyl group and the conjugated structure were decomposed at the third phase between 287 and 589 °C, indicating the thermal decomposition of PVA.

https://doi.org/10.1021/acsomega.2c05110
ACS Omega 2023, 8, 2915−2930

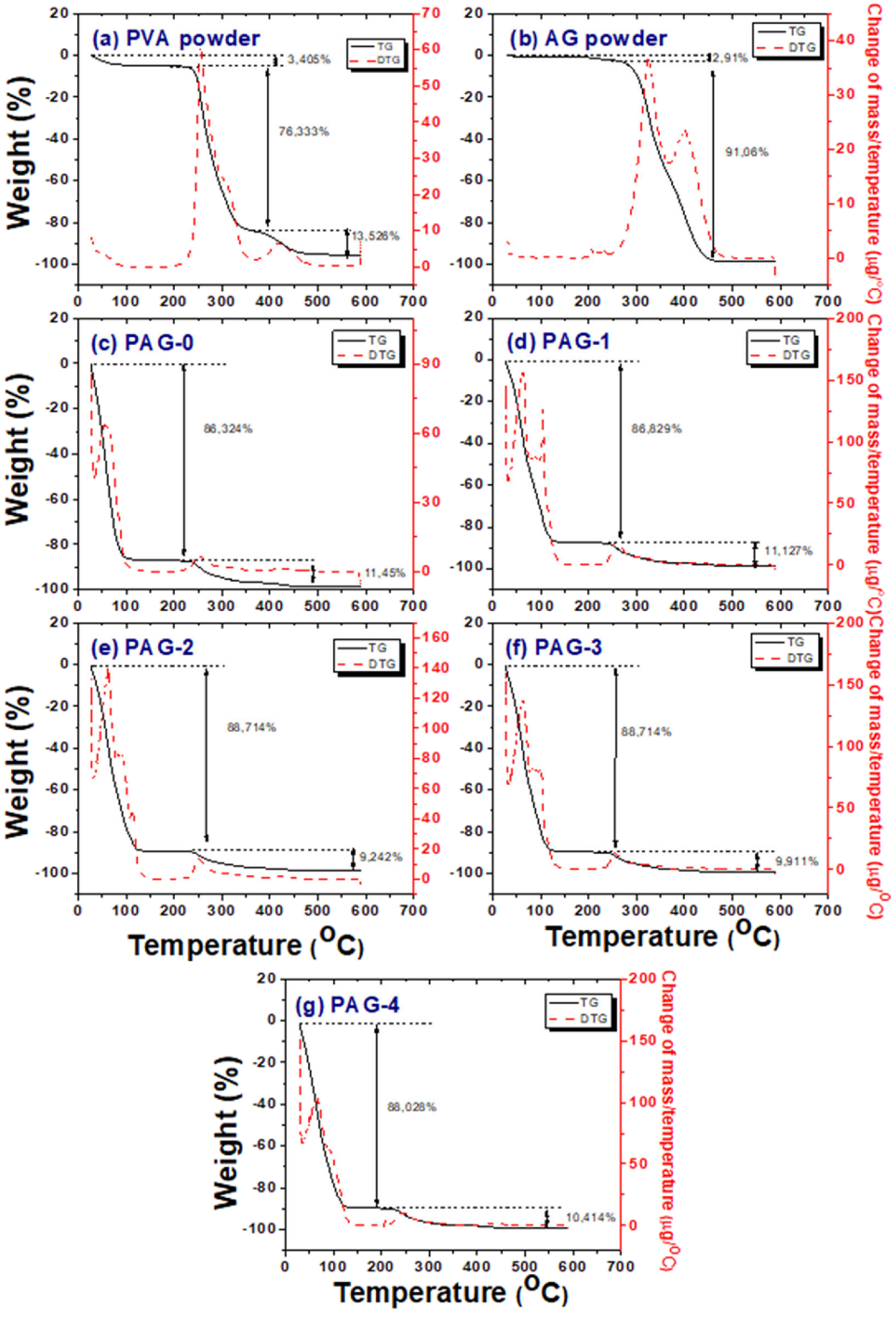

Figure 8. TG/DTG plots of (a) PVA powder, (b) AG powder, and PVA/AG hydrogels: (c) PAG-0, (d) PAG-1, (e) PAG-2, (f) PAG-3, and (g) PAG-4.

The residue of the PVA powder at the end of the measurement was about 4.2%, which indicates the presence of inorganic compounds in the sample with a small fraction of impurities.[82] Additionally, the AG powder decomposition has been studied previously:[83] AG underwent a significant weight reduction (96.01%) at temperatures around 300−473 °C. The decomposition peaks occurred at 324 and 402 °C, with a relatively small residue of 1.08% at 600 °C, because the AG powder is a pure crystal compound, as confirmed by the XRD results. As shown in Table 3, all the PVA/AG hydrogel samples show relatively small residues at 600 °C due to the presence of AG, which has a small residual value.

For the PVA/AG hydrogel samples, the curve shows a significant reduction in weight during the initial heating phase

https://doi.org/10.1021/acsomega.2c05110
ACS Omega 2023, 8, 2915−2930

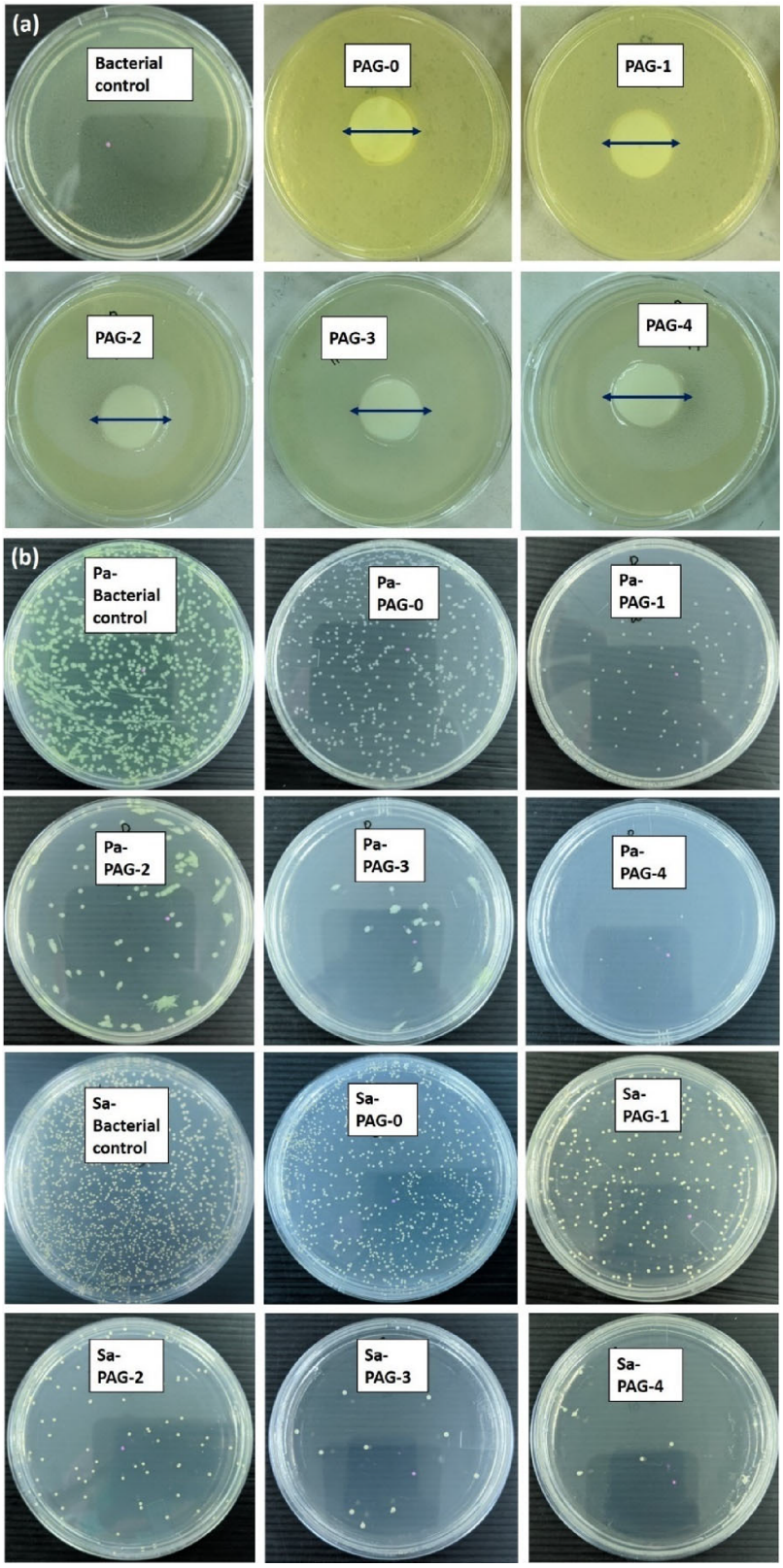

Figure 9. (a) Inhibition zone of bacterial activity; (b) bacteria colonies in the PVA/AG hydrogels: *Pseudomonas aeruginosa* (Pa) and *Staphylococcus aureus* (Sa).

due to the water and ethanol evaporation in the hydrogel.[32] A liquid/water evaporation phase and a hydrogel solid breakdown phase are the two stages of the hydrogel samples' decomposition process. From 30 to 120 °C, the liquid/water content in the hydrogel network began to evaporate. All hydrogel samples lost weight due to this evaporation by more than 80% because they contained a lot of fluid.

https://doi.org/10.1021/acsomega.2c05110
ACS Omega 2023, 8, 2915−2930

In the next phase, the hydrogel solids' decomposition occurred when they lost their liquid at temperatures between 230 and 600 °C. During the decomposition process, the loss of the hydroxyl groups and the main chain (−CH) resulted in weight loss in this phase between 9% and 11%.[15] Thus, the hydrogel PAG-0 experienced the largest shrinkage by 11.45%.

3.7. Antibacterial Activity. Figure 9a depicts the inhibition zone around the hydrogel samples in the antibacterial test against *Pseudomonas aeruginosa* and *Staphylococcus aureus*. In this experiment, the hydrogels PAG-0 to PAG-4 with a diameter of each sample of about 22 mm were weighed and then examined for their inhibition zones. After 24 h of incubation, the inhibition zone against *Pseudomonas aeruginosa* and *Staphylococcus aureus* bacteria was formed as indicated by a clear area around the samples. However, the zone was difficult to observe clearly since the samples had a similar color to the agar test medium. Therefore, a subsequent test was conducted to confirm the antibacterial activity of the PVA/AG hydrogels. The total plate count (TPC) test was carried out to obtain a more quantitative result in determining the reduction of bacteria around the samples.[84]

Figure 9b depicts the number of bacteria colonies determined by the TPC test. After incubation, the number of bacterial colonies for control and all hydrogel samples was counted using a colony counter to determine the antibacterial activity.[32] The antibacterial activity analyzed by eq 4, which is shown in Table 4, informed that the PVA hydrogel surprisingly had some antibacterial activity based on these results. The antibacterial activity of the PVA hydrogel is thought to be due to water diffusion out of the hydrogel, which disrupted bacterial reproduction on the agar plate. When water flows outward from PVA hydrogels, it has a pushing force that disrupts bacterial populations away from the peripheral of the hydrogel.[14] Table 4 shows that the antibacterial activity of the hydrogels increased with increasing AG concentration, which resulted in a reduction in the number of bacterial colonies in both types of bacteria. The addition of AG in the antibacterial activity of *Staphylococcus aureus* had no significant difference for all samples ($p > 0.05$). For *Pseudomonas aeruginosa*, the antibacterial activity for PAG-4 had a significant difference with the rest of the samples ($p < 0.05$). However, there was no significant difference between groups for the PAG-0, PAG-1, PAG-2, and PAG-3 ($p > 0.05$).

Table 4. Antibacterial Activity of PVA/AG Hydrogels

	Pseudomonas aeruginosa		*Staphylococcus aureus*	
sample	bacterial colonies (cfu/mL)	antibacterial activity (%/g)	bacterial colonies (cfu/mL)	antibacterial activity (%/g)
PAG-0	11.8 ± 0.1^{a}	10.4 ± 0.1^{a}	11.8 ± 0.1^{b}	3.5 ± 0.5^{a}
PAG-1	11.4 ± 0.6^{a}	14.5 ± 0.1^{a}	10.7 ± 0.9^{ab}	3.7 ± 0.5^{a}
PAG-2	11.2 ± 0.3^{a}	14.6 ± 0.6^{a}	10.4 ± 0.1^{ab}	5.0 ± 5.2^{a}
PAG-3	10.8 ± 0.2^{a}	15.3 ± 0.5^{a}	10.1 ± 0.1^{a}	7.3 ± 1.7^{a}
PAG-4	10.8 ± 0.1^{a}	37.9 ± 4.6^{b}	9.9 ± 0.1^{a}	8.2 ± 0.1^{a}
Control	1.4 ± 0.3^{b}		14.4 ± 0.3^{c}	

As confirmed in the previous study,[19] AG possesses an antibacterial activity; hence the highest antibacterial activity is the composite hydrogel that has the highest AG content. The PAG-4 hydrogel shows the highest antibacterial activity against *Pseudomonas aeruginosa* (37.9 ± 4.6^{b} %) and *Staphylococcus aureus* (8.2 ± 0.1^{a} %). The antibacterial activity against *Pseudomonas aeruginosa* (Gram-positive bacteria) was greater than *Staphylococcus aureus* (Gram-negative bacteria). Previous studies suggest that Gram-positive bacteria are more sensitive to a bioactive compound (AG) than Gram-negative bacteria.[85,86] *Staphylococcus aureus* is generally more resistant to AG because they have an outer membrane with a larger periplasmic area than *Pseudomonas aeruginosa*, which have almost no periplasmic area.[87] This result indicates that the highest antibacterial activity (PAG-4) at a concentration of 0.4% AG powder or with a weight ratio (AG and PVA powder) of 0.008:1 showed almost the same antibacterial activity as a natural extract/PVA hydrogel whose weight ratio is much higher (0.5:1).[15] The results are also similar to the previous study in that the use of bioactive compounds in a small ratio into the PVA hydrogel (0.0025:1) showed antibacterial activity for wound dressing application.[13] The periplasmic zone in *Staphylococcus aureus* is up to 40% of the total cell volume of Gram-negative bacteria.[88] This result shows that the PVA/AG hydrogel has an antibacterial ability against both types of bacteria, which can potentially be used as antibacterial applications such as in contact lenses, dental infections, tissue engineering, prosthesis implant infections, gastrointestinal infections, and wound dressing applications.[84] These applications require a hydrogel with high antibacterial activity, which aims to prevent the possibility of bacteria entering the body and inhibiting the growth of bacteria into the body. The ability of hydrogels to break the bacterial membranes is useful to inhibit bacterial growth; hence, it can treat infections in the body effectively.[84]

4. CONCLUSIONS

PVA/AG hydrogels of varying compositions of AG have been successfully produced using the freeze−thaw method. The analysis of the SEM images indicates the increase of the pore size with increasing AG because AG interfered with the hydroxyl group formation process in PVA and decreased the formation of cross-links between chains. This result was confirmed by the tests of porosity and compressive strength. The PVA/AG hydrogels had maximum swelling degrees above 100%, while the presence of AG significantly reduced the degree of swelling. PVA and AG were present in PVA/AG hydrogels, as observed in the FTIR spectra. The amorphization of AG in the PVA/AG hydrogels was shown by the XRD pattern, and the decrease of the melting temperature was confirmed by the TG/DSC characterization. The antibacterial activity of PVA/AG increased with the increase of AG concentration. The PAG-4 hydrogel had the highest antibacterial activity against *Pseudomonas aeruginosa* at 37.9 ± 4.6^{b} % and *Staphylococcus aureus* at 8.2 ± 0.1^{a} %. These tests show that the PVA/AG hydrogel could potentially be used in antibacterial applications since it has an antibacterial ability against both Gram-positive and Gram-negative bacteria.

AUTHOR INFORMATION

Corresponding Author

Khairurrijal Khairurrijal − *Department of Physics, Faculty of Mathematics and Natural Sciences, Institut Teknologi Bandung, Bandung 40132 Jawa Barat, Indonesia; Bioscience and Biotechnology Research Center, University Center of Excellence for Nutraceuticals, Institut Teknologi Bandung, Bandung, Jawa Barat 40132, Indonesia; Department of Physics, Faculty of Science, Institut Teknologi Sumatera,*

https://doi.org/10.1021/acsomega.2c05110
ACS Omega 2023, 8, 2915−2930

Lampung Selatan 35365, Indonesia; orcid.org/0000-0002-9452-4192; Email: krijal@itb.ac.id

Authors

Halida Rahmi Luthfianti − *Doctoral Program of Physics, Faculty of Mathematics and Natural Sciences and Department of Physics, Faculty of Mathematics and Natural Sciences, Institut Teknologi Bandung, Bandung 40132 Jawa Barat, Indonesia*

William Xaveriano Waresindo − *Doctoral Program of Physics, Faculty of Mathematics and Natural Sciences and Department of Physics, Faculty of Mathematics and Natural Sciences, Institut Teknologi Bandung, Bandung 40132 Jawa Barat, Indonesia*

Dhewa Edikresnha − *Department of Physics, Faculty of Mathematics and Natural Sciences, Institut Teknologi Bandung, Bandung 40132 Jawa Barat, Indonesia; Bioscience and Biotechnology Research Center, University Center of Excellence for Nutraceuticals, Institut Teknologi Bandung, Bandung, Jawa Barat 40132, Indonesia;* orcid.org/0000-0001-6203-4343

Agus Chahyadi − *Bioscience and Biotechnology Research Center, University Center of Excellence for Nutraceuticals, Institut Teknologi Bandung, Bandung, Jawa Barat 40132, Indonesia;* orcid.org/0000-0002-3625-4577

Tri Suciati − *Department of Pharmaceutics, School of Pharmacy, Institut Teknologi Bandung, Bandung, Jawa Barat 40132, Indonesia*

Fatimah Arofiati Noor − *Department of Physics, Faculty of Mathematics and Natural Sciences, Institut Teknologi Bandung, Bandung 40132 Jawa Barat, Indonesia*

Complete contact information is available at: https://pubs.acs.org/10.1021/acsomega.2c05110

Author Contributions

H.R.L. contributed to conceptualization, methodology, writing-original draft, and data curation. W.X.W. contributed to conceptualization, methodology, and data curation. D.E. contributed to resources and supervision. A.C. contributed to resources and data curation. T.S. contributed to resources and supervision. F.A.N, contributed to resources, editing, and supervision. K.K. contributed to resources, writing−review, editing, supervision, and funding acquisition.

Notes

The authors declare no competing financial interest.

■ ACKNOWLEDGMENTS

This research was financially supported by the Directorate of Research and Community Engagement, Institut Teknologi Bandung, under the "ITB Research Program" (Program Riset ITB) Grant in the fiscal years of 2020-2021. H.R.L. acknowledges the Ganesha Talent Assistantship Research Group (GTA-RG) for the provision of the doctoral scholarship. W.X.W. acknowledges the Indonesian Endowment Fund for Education (LPDP) for the provision of the doctoral scholarship. The authors would like also to thank Basic Science Center A, Faculty of Mathematics and Natural Sciences, ITB, for conducting SEM characterization.

■ REFERENCES

(1) Varaprasad, K.; Raghavendra, G. M.; Jayaramudu, T.; Yallapu, M. M.; Sadiku, R. A Mini Review on Hydrogels Classification and Recent Developments in Miscellaneous Applications. *Mater. Sci. Eng., C* **2017**, *79*, 958−971.

(2) Gyles, D. A.; Castro, L. D.; Silva, J. O. C., Jr.; Ribeiro-Costa, R. M. A review of the designs and prominent biomedical advances of natural and synthetic hydrogel formulations. *Eur. Polym. J.* **2017**, *88*, 373−392.

(3) Teodorescu, M.; Bercea, M.; Morariu, S. Biomaterials of poly (vinyl alcohol) and natural polymers. *Polym. Rev.* **2018**, *58*, 247−287.

(4) Mahinroosta, M.; Farsangi, Z. J.; Allahverdi, A.; Shakoori, Z. Hydrogels as intelligent materials: A brief review of synthesis, properties and applications. *Mater. Today Chem.* **2018**, *8*, 42−55.

(5) Gu, L.; Mooney, D. J. Biomaterials and emerging anticancer therapeutics: Engineering the microenvironment. *Nat. Rev. Cancer* **2016**, *16*, 56−66.

(6) Yokoyama, F.; Masada, I.; Shimamura, K.; Ikawa, T.; Monobe, K. Morphology and structure of highly elastic poly (vinyl alcohol) hydrogel prepared by repeated freezing-and-melting. *Colloid Polym. Sci.* **1986**, *264*, 595−601.

(7) Holloway, J. L.; Lowman, A. M.; Palmese, G. R. The role of crystallization and phase separation in the formation of physically cross-linked PVA hydrogels. *Soft Matter* **2013**, *9*, 826−833.

(8) Zhang, W.; Chen, H.; Wang, J.; Wang, Y.; Xing, L.; Zhang, H. Physicochemical properties of three starches derived from potato, chestnut, and yam as affected by freeze-thaw treatment. *Starch/Staerke* **2014**, *66*, 353−360.

(9) Li, X.; Jiang, Y.; Wang, F.; Fan, Z.; Wang, H.; Wang, Z. Preparation of polyurethane/polyvinyl alcohol hydrogel and its performance enhancement *via* compositing with silver particles. *RSC Adv.* **2017**, *7*, 46480−46485.

(10) Kamoun, E. A.; Kenawy, E. R. S.; Chen, X. A review on polymeric hydrogel membranes for wound dressing applications: PVA-based hydrogel dressings. *J. Adv. Res.* **2017**, *8*, 217−233.

(11) Grinstaff, M. W. Designing hydrogel adhesives for corneal wound repair. *Biomaterials* **2007**, *28*, 5205−5214.

(12) Sriyanti, I.; Edikresnha, D.; Rahma, A.; Munir, M. M.; Rachmawati, H.; Khairurrijal, K. Correlation between Structures and Antioxidant Activities of Polyvinylpyrrolidone/*Garcinia mangostana* L. Extract Composite Nanofiber Mats Prepared Using Electrospinning. *J. Nanomater.* **2017**, *2017*, No. 9687896.

(13) Kim, M.-S.; Oh, G.-W.; Jang, Y.-M.; Ko, S.-C.; Park, W.-S.; Choi, I.-W.; Kim, Y.-M.; Jung, W.-K. Antimicrobial hydrogels based on PVA and diphlorethohydroxycarmalol (DPHC) derived from brown alga Ishige okamurae: An in vitro and in vivo study for wound dressing application. *Mater. Sci. Eng., C* **2020**, *107*, No. 110352.

(14) Edikresnha, D.; Suciati, T.; Suprijadi; Khairurrijal, K. Freeze-Thawed Hydrogel Loaded by Piper crocatum Extract with In-Vitro Antibacterial and Release Tests. *J. Mater. Res. Technol.* **2021**, *15*, 17−36.

(15) Waresindo, W. X.; Luthfianti, H. R.; Edikresnha, D.; Suciati, T.; Noor, F. A.; Khairurrijal, K. A freeze−thaw PVA hydrogel loaded with guava leaf extract: physical and antibacterial properties. *RSC Adv.* **2021**, *11*, 30156−30171.

(16) Eakwaropas, P.; Ngawhirunpat, T.; Rojanarata, T.; Akkaramongkolporn, P.; Opanasopit, P.; Patrojanasophon, P. Fabrication of electrospun hydrogels loaded with Ipomoea pes-caprae (L.) R. Br extract for infected wound. *J. Drug Delivery Sci. Technol.* **2020**, *55*, No. 101478.

(17) Sriyanti, I.; Marlina, L.; Fudholi, A.; Marsela, S.; Jauhari, J. Physicochemical properties and in vitro evaluation studies of polyvinylpyrrolidone/cellulose acetate composite nanofibres loaded with Chromolaena odorata (L) King extract. *J. Mater. Res. Technol.* **2021**, *12*, 333−342.

(18) Juby, K. A.; Dwivedi, C.; Kumar, M.; Kota, S.; Misra, H. S.; Bajaj, P. N. Silver nanoparticle-loaded PVA/gum acacia hydrogel: Synthesis, characterization and antibacterial study. *Carbohydr. Polym.* **2012**, *89*, 906−913.

(19) Aromdee, C.; Sriubolmas, N.; Wiyakrutta, S.; Suebsasna, S.; Khunkitti, W. Effect of the derivatives of andrographolide on the

morphology of Bacillus subtilis. *Arch. Pharmacal Res.* **2011**, *34*, 71−77.
(20) Elfahmi; Woerdenbag, H. J.; Kayser, O. Jamu: Indonesian traditional herbal medicine towards rational phytopharmacological use. *J. Herb. Med.* **2014**, *4*, 51−73.
(21) Lattoo, S. K.; Dhar, R. S.; Khan, S.; Bamotra, S.; Bhan, M. K.; Dhar, A. K.; Gupta, K. K. Comparative analysis of genetic diversity using molecular and morphometric markers in Andrographis paniculata (Burm. f.) Nees. *Genet. Resour. Crop Evol.* **2008**, *55*, 33−43.
(22) Banerjee, M.; Parai, D.; Chattopadhyay, S.; Mukherjee, S. K. Andrographolide: antibacterial activity against common bacteria of human health concern and possible mechanism of action. *Folia Microbiol.* **2017**, *62*, 237−244.
(23) Jiang, X.; Yu, P.; Jiang, J.; Zhang, Z.; Wang, Z.; Yang, Z.; Tian, Z.; Wright, S. C.; Larrick, J. W.; Wang, Y. Synthesis and evaluation of antibacterial activities of andrographolide analogues. *Eur. J. Med. Chem.* **2009**, *44*, 2936−2943.
(24) Yu, T.; Jiang, X.; Xu, X.; Jiang, C.; Kang, R.; Jiang, X. Andrographolide Inhibits Biofilm and Virulence in Listeria monocytogenes as a Quorum-Sensing Inhibitor. *Molecules* **2022**, *27*, 1−13.
(25) Zhang, L.; Bao, M.; Liu, B.; Zhao, H.; Zhang, Y.; Ji, X. Y.; Zhao, N.; Zhang, C.; He, X.; Yi, J.; Tan, Y.; Li, L.; Lu, C. Effect of Andrographolide and Its Analogs on Bacterial Infection: A Review. *Pharmacology* **2020**, *105*, 123−134.
(26) Chen, M.; Xie, C.; Liu, L. Solubility of andrographolide in various solvents from (288. 2 to 323.2) K. *J. Chem. Eng. Data* **2010**, *55*, 5297−5298.
(27) Fan, L.; Yang, H.; Yang, J.; Peng, M.; Hu, J. Preparation and characterization of chitosan / gelatin / PVA hydrogel for wound dressings. *Carbohydr. Polym.* **2016**, *146*, 427−434.
(28) Qiu, Y.; Park, K. Environment-sensitive hydrogels for drug delivery. *Adv. Drug Delivery Rev.* **2001**, *53*, 321−339.
(29) Lee, D.; Zhang, H.; Ryu, S. Elastic Modulus Measurement of Hydrogels. *Cellulose-Based Superabsorbent Hydrogel*; Elsevier 2019, 1−21. doi: DOI: 10.1007/978-3-319-77830-3_60.
(30) Ma, S.; Wang, S.; Li, Q.; Leng, Y.; Wang, L.; Hu, G.-H. A Novel Method for Preparing Poly(vinyl alcohol) Hydrogels : Preparation, Characterization, and Application. *Ind. Eng. Chem. Res.* **2017**, *56*, 7971−7976.
(31) Hassan, C. M.; Peppas, N. A. Structure and morphology of freeze/thawed PVA hydrogels. *Macromolecules* **2000**, *33*, 2472−2479.
(32) Edikresnha, D.; Suciati, T.; Munir, M. M.; Khairurrijal, K. Polyvinylpyrrolidone/cellulose acetate electrospun composite nanofibres loaded by glycerine and garlic extract with: In vitro antibacterial activity and release behaviour test. *RSC Adv.* **2019**, *9*, 26351−26363.
(33) Gupta, S.; Goswami, S.; Sinha, A. A combined effect of freeze-thaw cycles and polymer concentration on the structure and mechanical properties of transparent PVA gels. *Biomed. Mater.* **2012**, *7*, No. 015006.
(34) Tavakoli, J.; Gascooke, J.; Xie, N.; Tang, B. Z.; Tang, Y. Enlightening Freeze−Thaw Process of Physically Cross-Linked Poly(vinyl alcohol) Hydrogels by Aggregation-Induced Emission Fluorogens. *ACS Appl. Polym. Mater.* **2019**, *1*, 1390−1398.
(35) Stauffer, S. R.; Peppast, N. A. Poly (vinyl alcohol) hydrogels prepared by freezing-thawing cyclic processing. *Polymer (Guildf).* **1992**, *33*, 3932−3936.
(36) Trieu, H. H.; Qutubuddin, S. Polyvinyl alcohol hydrogels I. Microscopic structure by freeze-etching and critical point drying techniques. *Colloid Polym. Sci.* **1994**, *272*, 301−309.
(37) Kobayashi, M.; Kanekiyo, M.; Ando, I.; Amiya, S. A study of the gelation mechanism of poly(vinyl alcohol) in aqueous solution by high-resolution solid-state 13C NMR spectroscopy. *Polym. Gels Networks* **1998**, *6*, 425−428.
(38) Yamaura, K.; Kumakura, R. Gel-spinning of partially saponificated poly(vinyl alcohol). *J. Appl. Polym. Sci.* **2000**, *77*, 2872−2876.
(39) Zou, S.; Wei, Z.; Hu, Y.; Deng, Y.; Tong, Z.; Wang, C. Macroporous antibacterial hydrogels with tunable pore structures fabricated by using Pickering high internal phase emulsions as templates. *Polym. Chem.* **2014**, *5*, 4227−4234.
(40) Tao, G.; Wang, Y.; Cai, R.; Chang, H.; Song, K.; Zuo, H.; Zhao, P.; Xia, Q.; He, H. Design and performance of sericin / poly (vinyl alcohol) hydrogel as a drug delivery carrier for potential wound dressing application. *Mater. Sci. Eng., C* **2019**, *101*, 341−351.
(41) Guan, Y.; Bian, J.; Peng, F.; Zhang, X. M.; Sun, R. C. High strength of hemicelluloses based hydrogels by freeze/thaw technique. *Carbohydr. Polym.* **2014**, *101*, 272−280.
(42) Butylina, S.; Geng, S.; Oksman, K. Properties of as-prepared and freeze-dried hydrogels made from poly(vinyl alcohol) and cellulose nanocrystals using freeze-thaw technique. *Eur. Polym. J.* **2016**, *81*, 386−396.
(43) Ou, K.; Dong, X.; Qin, C.; Ji, X.; He, J. Properties and toughening mechanisms of PVA/PAM double-network hydrogels prepared by freeze-thawing and anneal-swelling. *Mater. Sci. Eng., C* **2017**, *77*, 1017−1026.
(44) Khorasani, M. T.; Joorabloo, A.; Adeli, H.; Mansoori-Moghadam, Z.; Moghaddam, A. Design and optimization of process parameters of polyvinyl (alcohol)/chitosan/nano zinc oxide hydrogels as wound healing materials. *Carbohydr. Polym.* **2019**, *207*, 542−554.
(45) Jaipakdee, N.; Pongjanyakul, T.; Limpongsa, E. Preparation and characterization of poly (vinyl alcohol)-poly (vinyl pyrrolidone) mucoadhesive buccal patches for delivery of lidocaine HCL. *Int. J. Appl. Pharm.* **2018**, *10*, 115−123.
(46) Syukri, Y.; Martien, R.; Lukitaningsih, E.; Nugroho, A. E. Quantification of Andrographolide Isolated from *Andrographis paniculata* Nees Obtained from Traditional Market in Yogyakarta Using Validated HPLC. *Indones. J. Chem.* **2016**, *16*, 190.
(47) Mansur, H. S.; Oréfice, R. L.; Mansur, A. A. P. Characterization of poly (vinyl alcohol)/poly (ethylene glycol) hydrogels and PVA-derived hybrids by small-angle X-ray scattering and FTIR spectroscopy. *Polymer* **2004**, *45*, 7193−7202.
(48) Chakraborty, S.; Biswas, S.; Sa, B.; Das, S.; Dey, R. *In vitro & in vivo* correlation of release behavior of andrographolide from silica and PEG assisted silica gel matrix. *Colloids Surf., A* **2014**, *455*, 111−121.
(49) Zheng, C.; Liu, C.; Chen, H.; Wang, N.; Liu, X.; Sun, G.; Qiao, W. Effective wound dressing based on Poly (vinyl alcohol)/Dextran-aldehyde composite hydrogel. *Int. J. Biol. Macromol.* **2019**, *132*, 1098−1105.
(50) Sirousazar, M.; Khodamoradi, P. Freeze-thawed humic acid/polyvinyl alcohol supramolecular hydrogels. *Mater. Today Commun.* **2020**, *22*, No. 100719.
(51) Hendrawan, H.; Khoerunnisa, F.; Sonjaya, Y.; Putri, A. D. Poly (vinyl alcohol)/glutaraldehyde/*Premna oblongifolia* merr extract hydrogel for controlled-release and water absorption application. *IOP Conf. Ser.: Mater. Sci. Eng.* **2019**, *509*, No. 012048.
(52) Sriyanti, I.; Edikresnha, D.; Rahma, A.; Miftahul Munir, M.; Rachmawati, H.; Khairurrijal, K. Mangosteen pericarp extract embedded in electrospun PVP nanofiber mats: physicochemical properties and release mechanism of α-mangostin. *Int. J. Nanomed.* **2018**, *13*, 4927−4941.
(53) Mustikasari, D.; Rezeki, Y. A.; Munir, M. M.; Rachmawati, H.; Khairurrijal, K. Turmeric extract-loaded polyvinylpyrrolidone spherical submicron particles produced using electrohydrodynamic atomization: their physico-chemical properties and antioxidant activity. *Mater. Res. Express* **2019**, *6*, No. 085415.
(54) Ahmadian, Y.; Bakravi, A.; Hashemi, H.; Namazi, H. Synthesis of polyvinyl alcohol/CuO nanocomposite hydrogel and its application as drug delivery agent. *Polym. Bull.* **2019**, *76*, 1967−1983.
(55) Rezeki, Y. A.; Hapidin, D. A.; Rachmawati, H.; Munir, M. M.; Khairurrijal, K. Formation of electrosprayed composite nanoparticles from polyvinylpyrrolidone / mangosteen pericarp extract. *Adv. Powder Technol.* **2020**, *31*, 1811−1824.
(56) Guan, Y.; Qi, X. M.; Zhang, B.; Chen, G. G.; Peng, F.; Sun, R. C. Physically crosslinked composite hydrogels of hemicelluloses with poly(vinyl alcohol phosphate) and chitin nanowhiskers. *BioResources* **2014**, *10*, 1378−1393.

https://doi.org/10.1021/acsomega.2c05110
ACS Omega 2023, 8, 2915−2930

(57) Li, W.; Wang, D.; Yang, W.; Song, Y. Compressive mechanical properties and microstructure of PVA-HA hydrogels for cartilage repair. *RSC Adv.* **2016**, *6*, 20166−20172.
(58) Wang, Y.; Xue, Y.; Wang, J.; Zhu, Y.; Zhu, Y.; Zhang, X.; Liao, J.; Li, X.; Wu, X.; Qin, Y. X.; Chen, W. A composite hydrogel with high mechanical strength, fluorescence, and degradable behavior for bone tissue engineering. *Polymers (Basel)* **2019**, *11*, 1112.
(59) Krupa, I.; Nedelčev, T.; Račko, D.; Lacík, I. Mechanical properties of silica hydrogels prepared and aged at physiological conditions: Testing in the compression mode. *J. Sol-Gel Sci. Technol.* **2010**, *53*, 107−114.
(60) Kim, T. H.; An, D. B.; Oh, S. H.; Kang, M. K.; Song, H. H.; Lee, J. H. Creating stiffness gradient polyvinyl alcohol hydrogel using a simple gradual freezing-thawing method to investigate stem cell differentiation behaviors. *Biomaterials* **2015**, *40*, 51−60.
(61) Figueroa-Pizano, M. D.; Vélaz, I.; Peñas, F. J.; Zavala-Rivera, P.; Rosas-Durazo, A. J.; Maldonado-Arce, A. D.; Martínez-Barbosa, M. E. Effect of freeze-thawing conditions for preparation of chitosan-poly (vinyl alcohol) hydrogels and drug release studies. *Carbohydr. Polym.* **2018**, *195*, 476−485.
(62) Wang, Y.; Marshall, K. L.; Baba, Y.; Gerling, G. J.; Lumpkin, E. A. Hyperelastic Material Properties of Mouse Skin under Compression. *PLoS One* **2013**, *8*, No. e67439.
(63) Tang, X.; Gu, X.; Wang, Y.; Chen, X.; Ling, J.; Yang, Y. Stable antibacterial polysaccharide-based hydrogels as tissue adhesives for wound healing. *RSC Adv.* **2020**, *10*, 17280−17287.
(64) Yu, Y.; Yuk, H.; Parada, G. A.; Wu, Y.; Liu, X.; Nabzdyk, C. S.; Youcef-Toumi, K.; Zang, J.; Zhao, X. Multifunctional " Hydrogel Skins " on Diverse Polymers with Arbitrary Shapes. *Adv. Mater.* **2019**, *31*, No. e1807101.
(65) Dourado, D. Thermal Analysis as a Useful Tool in Drug-Excipient Compatibilty Studies: The Impact in Pharmaceuticals Products. *Biomed. j. sci. technol. res.* **2019**, *22*, 16634−16636.
(66) Mazurek-Wadołkowska, E.; Winnicka, K.; Czajkowska-Kośnik, A.; Czyzewska, U.; Miltyk, W. Application of differential scanning calorimetry in evaluation of solid state interactions in tablets containing acetaminophen. *Acta Pol. Pharm.* **2013**, *70*, 787−793.
(67) Almafie, M. R.; Marlina, L.; Riyanto, R.; Jauhari, J.; Nawawi, Z.; Sriyanti, I. Dielectric Properties and Flexibility of Polyacrylonitrile / Graphene Oxide Composite Nanofibers. *ACS Omega* **2022**, *7*, 33087−33096.
(68) Shriver, D. F.; Atkins, P. W.; Langford, C. H. *Inorganic chemistry*; 5th ed.; Oxford University Press: Oxford, 1999.
(69) Patel, A. K.; Bajpai, R.; Keller, J. M. On the crystallinity of PVA / palm leaf biocomposite using DSC and XRD techniques. *Microsyst. Technol.* **2014**, *20*, 41−49.
(70) Gray, A. P. Polymer crystallinity determinations by DSC. *Thermochim. Acta* **1970**, *1*, 563−579.
(71) Keller, A. Morphology of Crystallizing Polymers. *Nature* **1952**, *169*, 913−914.
(72) Charles, E.; Carraher, J.; *Polymer chemistry*; Sixth Edit.; Lagowski, J. J., Ed.; Marcel Dekker Inc: New York, 2003. doi: DOI: 10.1016/B978-1-84569-741-9.50002-1.
(73) Gradišar Centa, U.; Mihelčič, M.; Bobnar, V.; Remškar, M.; Slemenik Perše, L. The Effect of PVP on Thermal, Mechanical, and Dielectric Properties in PVDF-HFP/PVP Thin Film. *Coatings* **2022**, *12*, 1241.
(74) Cheng, J.; Wang, S.; Chen, S.; Zhang, J.; Wang, X. Crystallization behavior and hydrophilicity of poly(vinylidene fluoride)/poly(methyl methacrylate)/poly(vinyl pyrrolidone) ternary blends. *Polym. Int.* **2012**, *61*, 477−484.
(75) Cao, J.-H.; Zhu, B.-K.; Xu, Y.-Y. Structure and ionic conductivity of porous polymer electrolytes based on PVDF-HFP copolymer membranes. *J. Membr. Sci.* **2006**, *281*, 446−453.
(76) Sengwa, R. J.; Choudhary, S.; Dhatarwal, P. Nonlinear optical and dielectric properties of TiO2 nanoparticles incorporated PEO/PVP blend matrix based multifunctional polymer nanocomposites. *J. Mater. Sci.: Mater. Electron.* **2019**, *30*, 12275−12294.
(77) Zhao, J.; Wang, W.; Ye, C.; Li, Y.; You, J. Gravity-driven ultrafast separation of water-in-oil emulsion by hierarchically porous electrospun Poly(L-lactide) fabrics. *J. Membr. Sci.* **2018**, *563*, 762−767.
(78) Doumeng, M.; Makhlouf, L.; Berthet, F.; Marsan, O.; Delbé, K.; Denape, J.; Chabert, F. A comparative study of the crystallinity of polyetheretherketone by using density, DSC, XRD, and Raman spectroscopy techniques. *Polym. Test.* **2021**, *93*, No. 106878.
(79) Lanyi, F. J.; Wenzke, N.; Kaschta, J.; Schubert, D. W. On the Determination of the Enthalpy of Fusion of α-Crystalline Isotactic Polypropylene Using Differential Scanning Calorimetry, X-Ray Diffraction, and Fourier- Transform Infrared Spectroscopy: An Old Story Revisited. *Adv. Eng. Mater.* **2020**, *22*, No. 1900796.
(80) Zhang, Y.; Hu, X.; Liu, X.; Dandan, Y.; Di, D.; Yin, T.; Zhang, S.; Tang, X. Dry state microcrystals stabilized by an HPMC film to improve the bioavailability of andrographolide. *Int. J. Pharm.* **2015**, *493*, 214−223.
(81) AlFannakh, H.; Arafat, S. S.; Ibrahim, S. S. Synthesis, electrical properties, and kinetic thermal analysis of polyaniline/polyvinyl alcohol-magnetite nanocomposites film. *IEEE J. Sel. Top. Quantum Electron.* **2019**, *26*, 347−359.
(82) Reguieg, F.; Ricci, L.; Bouyacoub, N.; Belbachir, M.; Bertoldo, M. Thermal characterization by DSC and TGA analyses of PVA hydrogels with organic and sodium MMT. *Polym. Bull.* **2020**, *77*, 929−948.
(83) Zhao, L.; Mitomo, H.; Zhai, M.; Yoshii, F.; Nagasawa, N.; Kume, T. Synthesis of Antibacterial PVA/CM-Chitosan blend Hydrogels with Electron Beam Irradiation. *Carbohydr. Polym.* **2003**, *53*, 439−446.
(84) Li, S.; Dong, S.; Xu, W.; Tu, S.; Yan, L.; Zhao, C.; Ding, J.; Chen, X. Antibacterial Hydrogels. *Adv. Sci* **2018**, *5*, No. 1700527.
(85) Majumdar, M.; Misra, T. K.; Roy, D. N. In vitro anti-biofilm activity of 14-deoxy-11,12-didehydroandrographolide from Andrographis paniculata against Pseudomonas aeruginosa. *Braz. J. Microbiol.* **2020**, *51*, 15−27.
(86) Polash, S. A.; Saha, T.; Hossain, M. S.; Sarker, S. R. Investigation of the Phytochemicals, Antioxidant, and Antimicrobial Activity of the Andrographis paniculata Leaf and Stem Extracts. *Adv. Biosci. Biotechnol.* **2017**, *08*, 149−162.
(87) Duffy, C. F.; Power, R. F. Antioxidant and antimicrobial properties of some Chinese plant extracts. *Int. J. Antimicrob. Agents* **2001**, *17*, 527−529.
(88) Seltmann, G.; Holst, O. *The Bacterial Cell Wall*; Springer: Berlin, 2002. doi: DOI: 10.1007/978-3-662-04878-8.

https://doi.org/10.1021/acsomega.2c05110
ACS Omega 2023, 8, 2915−2930